Reconnection acceleration in Saturn's dayside magnetodisc: a multicase study with Cassini

R. L. Guo[1,2], Z. H. Yao[2], N. Sergis[3,10], Y. Wei[1,11], D. Mitchell[4], E. Roussos[5], B. Palmaerts[2], W. R. Dunn[6], A. Radioti[2], L. C. Ray[7], A. J. Coates[6], D. Grodent[2], C. S. Arridge[7], P. Kollmann[4], N. Krupp[5], J. H. Waite[8], M. K. Dougherty[9], J. L. Burch[8], W. X. Wan[1]

1 Key Laboratory of Earth and Planetary Physics, Institute of Geology and Geophysics, Chinese Academy of Sciences, Beijing, China
2 Laboratoire de Physique Atmospherique et Planetaire, STAR institute, Universite de Liege, Liege, Belgium
3 Office for Space Research and Technology, Academy of Athens, Athens, Greece
4 Applied Physics Laboratory, Johns Hopkins University, Laurel, Maryland, USA
5 Max-Planck-Institute für Sonnensystemforschung, Göttingen, Germany
6 UCL Mullard Space Science Laboratory, Dorking, RH5 6NT, UK
7 Department of Physics, Lancaster University, Bailrigg, Lancaster LA1 4YB, UK
8 Southwest Research Institute, San Antonio, TX, United States
9 Faculty of Natural Sciences, Department of Physics, Imperial College, London, UK
10 Institute of Astronomy, Astrophysics, Space Applications and Remote Sensing, National Observatory of Athens, Athens
11 College of Earth Sciences, University of Chinese Academy of Sciences, Beijing, China

Abstract

Recently, rotationally driven magnetic reconnection was firstly discovered in Saturn's dayside magnetosphere (Guo et al. 2018). This newly confirmed process could potentially drive bursty phenomena at Saturn, i.e., pulsating energetic particles and auroral emissions. Using Cassini's measurements of magnetic fields and charged particles, we investigate particle acceleration features during three magnetic reconnection events observed in Saturn's dayside magnetodisc. The results suggest that the rotationally driven reconnection process plays a key role in producing energetic electrons (up to 100 keV) and ions (several hundreds of keV). In particular, we find that energetic oxygen ions are locally accelerated at all three reconnection sites. Isolated, multiple reconnection sites were recorded in succession during an interval lasting for much less than one Saturn rotation period. Moreover, a secondary magnetic island is reported for the first time at the dayside, collectively suggesting that the reconnection process is not steady and could be 'drizzle-like'. This study demonstrates the fundamental importance of internally driven magnetic reconnection in accelerating particles in Saturn's dayside magnetosphere, and likewise in the rapidly rotating Jovian magnetosphere and beyond.

Introduction

Magnetic reconnection is a fundamental physical process that converts energy and accelerates charged particles in cosmic, laboratory, and space plasma environments (Zweibel & Yamada 2009). Magnetic reconnection changes the magnetic topology of a system and can couple different plasma populations (Hesse et al. 2017). This process plays a pivotal role in driving the interaction between external interplanetary magnetic fields and internal planetary magnetic fields (Dungey 1961), as well as driving the plasma dynamics inside planetary magnetospheres (e.g., in the nightside planetary magnetotails (Arridge et al. 2016; Hones 1979)).

Direct evidence of magnetopause reconnection has been reported at Earth (Paschmann et al. 1979) and other planets such as Mercury (Slavin et al. 2009) and Saturn (McAndrews et al. 2008). In the nightside magnetotail of Earth and Mercury, magnetic reconnection is considered to release the nightside magnetic energy that is accumulated via dayside magnetopause reconnection and plasma circulation. Magnetic reconnection and its consequent production of plasmoids and secondary islands also play important roles on magnetic flux closure in the nightside of Saturn's magnetosphere (Arridge et al. 2016; Jackman et al. 2011).

The kronian and jovian magnetospheres are, however, significantly different from the terrestrial and hermean magnetospheres for two major reasons: 1) their magnetospheres rotate much more rapidly, 2) they have internal plasma sources from their rings and moons, which inject hot plasmas into the magnetosphere system. Internally produced plasma in rapidly rotating magnetic environments is radially transported outward (Bagenal et al. 2016), and causes the magnetosphere to attain a stretched magnetic field configuration, termed the magnetodisc. Similar to the terrestrial and hermean magnetospheres, magnetic reconnection at Jupiter and Saturn has also been identified at their magnetopauses and the magnetotails (Arridge et al. 2016; Badman et al. 2013; Huddleston et al. 1997; Masters 2017). Moreover, the magnetic reconnection process on the nightside of the giant planetary magnetospheres can be driven not only by solar wind energy, but also by internal energy, known as internally driven magnetic reconnection (Jackman et al. 2011; Kronberg et al. 2007; Vasyliunas 1983). By surveying magnetic measurements from Cassini-MAG instrument, Delamere et al. (2015) revealed that the reconnection indicator (i.e., negative signature of the B_θ magnetic component in Kronographic Radial-Theta-Phi (KRTP) coordinates, a spherical polar coordinates) could exist at all local times, including high probabilities of occurrence at the unexpected pre-noon sectors, and suggested that the reconnection processes were 'drizzle-like' that occur at small patchy regions. Plasma injection into Saturn's inner magnetosphere is also revealed to exist at all local times (Azari et al. 2018). Guo et al. (2018) directly confirmed the existence of magnetic reconnection in Saturn's dayside magnetodisc (i.e., well inside the magnetopause) by examining the reconnection-associated Hall current system and the reconnection acceleration plasma features (including electrons and ions). They showed that heavy ions were accelerated up to 600 keV by the dayside magnetodisc reconnection (DMR). Following the DMR signature, 1-hour pulsating energetic electrons were observed, while it is unclear whether the coexistence of DMR and pulsating energetic electrons is a coincidence or if the two processes are physically connected. The quasi-periodic energetic electron pulsation signatures have been reported in many studies at many local times (Mitchell et al. 2009; Palmaerts et al. 2016a; Roussos et al. 2016; Yates et al. 2016), and have been suggested to be relevant to the pulsating auroral emissions (Badman et al. 2015; Palmaerts et al. 2016b).

In this study, we identify three DMR events, and investigate the associated energetic particle features by using Cassini's multi-instrument measurements. We report details of energetic oxygen ions and electrons in the reconnection region. Pitch angle features of hot electrons are also analyzed for each reconnection process.

Cassini observations of reconnection events

We analyze magnetic field observations from the Cassini-MAG instrument (Dougherty et al. 2004), thermal ion and electron measurements with energy range up to 28 keV (electrons) and 50 keV (ions) from Cassini-CAPS/IMS/ELS (Young et al. 2004), and energetic (>18 keV (electrons) and > 27 keV (ions)) particle data from the Low-Energy Magnetospheric Measurements System (LEMMS) and the Ion and Neutral Camera (INCA) of the Magnetosphere Imaging Instrument (MIMI) (Krimigis et al., 2004). Hot electron pitch angle information is available by combining the *in-situ* magnetic field and particle data.

Reconnection diffusion region is the key region of the magnetic reconnection domain. However, this region is very small and dynamic, and it is very difficult to explore this with a spacecraft. From a realistic perspective, the negative B_θ signature is usually adopted as a simplified indicator of the magnetic reconnection, which can also effectually expose the reconnection diffusion region. We surveyed the Cassini data that collected from 2005 to 2012, and obtained 139 events that contains negative B_θ signatures inside the magnetosphere at the noon sector from 9 LT (Local Time) to 15 LT, with latitude inside 30 degrees. There are 33 events showing correlations between the negative B_θ signatures and the flux increases of the energetic oxygen ion, which is one of the most important species at Saturn. In this work, we identify 3 reconnection diffusion events from the 33 events, and investigate their Hall magnetic signatures and their ambient plasma features.

Event 1: 25 November 2005

Figure 1a shows magnetic field components in Kronographic Radial-Theta-Phi coordinates for 25 November 2005 between 11:40 UT and 13:40 UT. Figure 1b shows the magnetic field components in the X-line coordinate system (Arridge et al. 2016), which is a rectangular coordinate system that removes the bend-back effect of the magnetic field lines in magnetodisc. Figure 1c shows energetic electron differential flux from 18 keV to 832 keV measured by the MIMI-LEMMS instrument. Figure 1d shows the energy spectrogram of omni-directional hot electron flux measured by the

CAPS-ELS instrument, and Figures 1e-1g shows pitch angle distribution for electrons within three different energy ranges, i.e., from 50 eV to 500 eV, 500 eV to 3 keV, and 3 keV to 28 keV. As shown in Figure 1e-1g, the coverage of pitch angles during the whole period was poor, which is a common situation in Cassini's CAPS-ELS dataset, due to the limited field-of-view of the instrument. Figure 1h shows energetic ion (generally protons) differential flux from 27 keV to 4 MeV from MIMI-LEMMS instrument. Figure 1i shows the energy spectrogram for omnidirectional ion flux from CAPS-IMS instrument. Figure 1j shows the energetic oxygen differential flux from 46 keV to nearly 1 MeV from MIMI-INCA instrument.

Following the negative B_θ signature in Figure 1a (or positive B_Z component in Figure 1b) at ~ 12:13 UT and ~ 13:10 UT, two magnetic reconnection sites (highlighted in pink) were detected by Cassini in the pre-noon sector (at 9 LT) at a radial distance of ~21 R_S (Saturn's Radius, 1R_S = 60, 268 km) from Saturn's center. Moreover, B_Y changes sign when B_Z reverses, which is consistent with reconnection-produced Hall magnetic fields (Arridge et al. 2016; Guo et al. 2018). As suggested by the correspondingly small $|B_r|$, the spacecraft was in the outflow part of the reconnection region when the negative B_θ was detected.

The electron spectrograms (Figure 1d) in the reconnection regions are featured by higher than the ambient plasma energies. The background region (before the highlighted intervals) where electrons have a wide energy region from 10s of eV to ~ 1 keV, while electrons in the reconnection sites are mostly from 100s to a few keV. The pitch angle distributions in Figure 1e-1g showed that the electrons in these reconnection sites are approximately isotropic, but are field-aligned outside the reconnection regions. The isotropic pitch angle distribution of electrons is a typical feature of magnetic reconnection outflow region (e.g., Wang et al. (2016)).

The energetic electron flux (in Figure 1c) is enhanced during the two negative B_θ intervals and is also correlated to the magnitude of the B_r component. When $|B_r|$ > 3 nT, the electron flux in both Figure 1c and 1d minimizes, suggesting that the spacecraft was away from the current sheet center. Before the second highlighted region, the energetic electron flux is also increased when $|B_r|$ decreases, suggesting that the reconnection processes have been proceeding for a while and the accelerated electrons have filled in the current sheet. In addition, as shown in Figure 1d, the central energy of the electron flux in the second reconnection site is higher than that in the first one. Moreover, the fluxes of energetic protons (tens of keV to >100 keV, shown in Figure 1h) and energetic oxygen ions (> 200 keV, shown in Figure 1j) are mainly enhanced in the second reconnection site. The enhancement of thermal ions (<10 keV) in the first reconnection site can be clearly seen in the ion spectrogram in Figure 1i. The two reconnection events detected nearby have significantly different accelerating features might suggest that they are two individual reconnection sites, and therefore it is consistent with the "drizzle-like" reconnection picture.

Event 2: 15 September 2008

Figure 2 shows the second event occurred on 15 September 2008 between 11:00 UT and 16:00 UT, in the near-noon sector (at 11.2 LT) and at a radial distance of ~18 R_S. The large magnitude of the B_r component was expected since Cassini was at high latitudes, similar to the case in Guo et al. (2018), implying that the spacecraft was in the outer layer of the current sheet. The negative B_θ signature in Figure 2a lasted for more than 2 hours from ~ 11:43 UT to ~14:24 UT and is followed by a bipolar B_θ signature around 14:53 UT.

The distinct structure at around 14:53 UT is likely a secondary island (highlighted in pink) inside the long-lasting negative B_θ interval. Additionally, in the X-line coordinates (Figure 2b), the bipolar signature of B_Y component is consistent with the Hall magnetic fields. The perpendicular flux of hot electrons is enhanced in the positive B_θ region of the secondary island (Figures 2e and 2f), while it is field-aligned in the rest of the long-lasting negative B_θ region. There is no signature in Figure 2d to show that electrons are substantially accelerated inside the secondary island, suggesting that this secondary island is not contracting. This is because that contracting secondary island would strongly energize electrons (Drake et al. 2006). The energetic oxygen flux (Figure 2j) enhances ahead of the encounter with the secondary island, while the energetic electron flux (Figure 2c) increases after the encounter with the positive B_θ region of the secondary island and keeps a high level outside the secondary island, which might be originated from other nearby secondary reconnection sites that generated the secondary island.

Besides the secondary island region, the energetic oxygen flux also enhances at the onset of the long-lasting negative B_θ region (marked by the first arrow in Figure 2a) and at the end of the negative B_θ region (marked by the second arrow in Figure 2a). After ~15:30 UT, while the energetic electrons flux increases sharply (marked by the black arrow in Figure 2c), the electron spectrogram in Figure 2d broadens to contain electrons with energy less than 100 eV. The pitch-angle for the broadband electron spectrogram is largely enhanced at perpendicular (Figures 2e and 2f), opposite to the bi-directional feature during the negative B_θ interval. The pitch-angle distributions of this event are different to those of the first event where the electrons showed much isotropic features in the negative B_θ region while bi-directional in the background. In the event of Figure 2, bi-directional electrons are seen also in the negative B_θ region. The difference between the two events might be due to the relative positions between Cassini and the current sheet, as the spacecraft's latitude in the second event was much higher than that in the first event. Hence, Cassini may be detecting the outer edge of the current sheet, which could have different plasma characteristics compared to the current center. It could also be due to aperiodic short time scale dynamics that often dominate locally.

Event 3: 15 April 2008

The third reconnection event was also observed in the near-noon sector (at 11.5

LT) with a radial distance of ~23 R_S. Figure 3 is organized in same manner as Figure 1 and 2, and shows data from 14 April 2008 21:40 UT to 15 April 2008 01:40 UT. There is a short negative B_θ region (transient 1) around 14 April 2008 23:15 UT (dashed vertical line). After transient 1, the B_θ component shows a significant bipolar signature (transient 2) with oscillations between 14 April 23:47 UT to 15 April 00:33 UT (highlighted in pink).

In transient 2, the corresponding Hall magnetic field is obvious in Figure 3b where the B_Y component reverses from positive to negative. In Figure 3f, the electrons with energies from 500 eV to 3 keV in this interval are enhanced both in the perpendicular and antiparallel directions (we lack parallel information due to the instrument's limited field of view), suggesting that this could be the electron exhaust region, which is the inner part of the reconnection region and is filled by energized electrons that have been accelerated by both the X-line and a parallel potential near the separatrix region (e.g., Egedal et al. (2012) and Wang et al. (2016)).

The energetic electron flux in Figure 3c is enhanced when B_θ attained large positive values during transient 2. The energetic oxygen flux increases on both sides of the B_θ bipolar interval and drops at the same time that the energetic electrons are suddenly enhanced. Considering that the electron diffusion region is much smaller than and is surrounded by the oxygen diffusion region, the features of energised plasma can suggest that the spacecraft moved from the oxygen diffusion region on the outer part of the reconnection region (the first oxygen flux enhancement during the transient 2), to the electron exhaust further inside the reconnection region (the oxygen flux decrease and meanwhile electron flux enhancement during the transient 2), and then back to the oxygen diffusion region (the second Oxygen flux enhancement during the transient 2).

In transient 1, the B_φ component was nearly zero before B_θ becomes negative, suggesting the azimuthal bend-back configuration of the magnetodisc (Vasyliunas 1983) is mostly eliminated by the reconnection process in this region. Revealed by the plasma properties, the reconnection signatures observed at transient 1 can be divided into three regions, which are indicated above Figure 3d with three horizontal arrows.

The first region is where the energetic oxygen and proton fluxes were enhanced, in Figures 3j and 3h, respectively. The electron spectrogram (Figure 3d) shows a cavity in the low energy range. Electrons with energy around 1 keV display a bi-directional pitch angle distribution (Figure 3f), but they are more isotropic above 3 keV (Figure 3g). The second region is after the cold electron cavity and before the peak of B_θ component. The energetic electron flux in Figure 3c was sharply enhances in this region. The electron spectrogram has two bands. The low energy band is associated with bi-directional features (Figure 3e), and the high-energy band is roughly isotropic (Figure 3f). The third region is where the B_θ component sharply drops to negative. The electron spectrogram here is again bimodal. The flux of low energy electron band is enhanced in the perpendicular direction (Figure 3e).

The double electron bands in transient 1 are likely the mixture of reconnection accelerated population and ambient population. Enhancements in the low energy electron band are correlated with the dips in B_r. The four groups of colored arrows above Figures 3a and 3d show the correspondence between the B_r dips and intensifications in the low energy electron bands. This correlation strongly indicates that the low energy electron population could only exist in the inner current sheet, while high energy electron population could reach to distances farther from the current sheet center (Sergis et al. 2011). The electron population in this event appeared to have different characteristics compared to the other two events presented in this work. A further statistical study of the electron properties at different radial distances, local times and latitudes is required to systematically understand the variable behavior of electrons in different events.

Discussion and conclusion

As suggested by Delamere et al. (2015), magnetic reconnection can be expected to occur at any local time and not only in the midnight sector. The unambiguous ion diffusion region reported by Guo et al. (2018) and the three reconnection cases in this study, provide additional and direct evidence of the existence of the dayside magnetodisc reconnection processes, which locally produce energetic electrons and ions with energies of 100s of keV at the dayside magnetosphere.

Figure 4 shows the line plots and the energy spectrograms for the flux of energetic hydrogen (top two panels) and oxygen (bottom two panels) during the enhancement in the first event studied here (the second highlighted region in Figure 1). The flux peaks across all the energies of the hydrogens and oxygens ions at the same time, eliminating the possibility that our signatures were generated by an injection event and suggesting that the ions were locally accelerated. The spectrograms is similar to that reported in Angelopoulos et al. (2008) for a terrestrial magnetotail reconnection event. It is readily expected that the flux would enhance (drop) when moving towards (away from) the reconnection region, since the magnetic reconnection domain is the source region of energetic particles.

Observational features from the three events support the concept of 'drizzle-like' reconnection process, i.e. reconnection on global scales facilitated through numerous, small-scale reconnection channels (Delamere et al. 2015). For the event on November 25, 2005 (Figure 1), the energy of the hot electrons in the second reconnection site is higher than the first one (Figure 1d). Furthermore, the >10 keV energetic ions prominently appear in the second reconnection site, while it was much quiet in the first one (Figures 1h and 1j). These difference between the accelerated particles suggests that the two detected reconnection signatures are not from the same reconnection site, indicating that Cassini sampled adjacent but independent reconnection channels, a signature consistent with the 'drizzle' concept that suggested by Delamere et al. (2015). In addition, the separation of the two reconnection sites in the azimuthal direction was ~ 12 R_S, if considering that they corotate with the magnetosphere (Yao et al. 2017) in the duration over one hour (the time gap of the two reconnection events). The large separation between the two reconnection regions may exclude the possibility that they come from different evolution stages of the same event. For the event on 15 September 2008 (Figure 2), there is a long-lasting negative B_θ interval. However, because of the lack of the information on the magnetic structure near the current sheet center, it is hard to determine whether the aforementioned negative B_θ signature is caused by one or more reconnection sites. The B_Y signatures are not consistent with the Hall magnetic field signatures outside the negative B_θ regions. This could either be due to the disturbed current sheet, that can result in the X-line coordinates failing to adequately represent the magnetic geometry near the reconnection region, which is very possible near the current sheet center where the magnetic strength is small; or be due to the interference from the nearby reconnection site if the reconnection process was 'drizzle-like'.

The three events show very diverse forms of plasma acceleration, which is naturally expected due to the temporal variations and differences along the Cassini trajectories in crossing the complex magnetic reconnection sites in giant planetary magnetospheres. The presence of oxygen ions throughout the magnetosphere introduces an additional layer to the reconnection site, forming an oxygen diffusion region outside the proton diffusion region. This added layer makes the ion diffusion region enlarged and more complex, as particles exhibit different behavior across diffusion regions. For instance, the energetic oxygen ions concentrate in a narrow angular range within the 90 x 120 degree field-of-view of MIMI-INCA and peak at the pitch angles neither parallel nor perpendicular, while protons present more isotropic features (not shown, informed from MIMI-INCA). The non-gyrotropic and anisotropic feature of the oxygen ions may be due to their non-frozen-in behavior during the acceleration in the diffusion region for their larger gyro-radii (Sergis et al. 2013) comparing to the protons. The efficient perpendicular acceleration on heavy ions has been revealed by Galileo in Jovian magnetotail reconnection region (Radioti et al. 2007). Combining with reconnection's parallel acceleration, it is therefore possible to have accelerated energetic heavy ions at a pitch angle between parallel and perpendicular as observed in our events. Additionally, the existence of the secondary island in the second event, suggests the reconnection process is not steady, which will increase the diversity in particle behavior. The reason for the double bands in the electron spectrogram in Figure 3d and their variation might be very complex as the reconnection can couple different populations (Hesse et al. 2017). We expect this coupling to be more pronounced for 'drizzle' reconnection, where multiple plasma populations can be mixed on small spatial scales over a broad magnetospheric region.

In summary, we detailed characteristics of plasma acceleration for three magnetic reconnection events located in the dayside magnetodisc of Saturn. The heavy ions have strong influence on the evolution of the magnetic reconnection (Liang et al. 2017). Since the content of heavy ions are fundamentally different in giant planets and Earth (Blanc et al. 2015), we would expect a different role of the heavy ions in triggering reconnection process at Saturn and the Earth's magnetospheres. Unsteady and 'drizzle-like' DMR processes at Saturn can energize particles and provide an energy source for exciting auroral emissions connected to Saturn's dayside polar region. Furthermore, if these processes are common and more energetic in Jupiter's magnetosphere, they may offer a crucial means for energizing the heavy ions that precipitate into Jupiter's atmosphere, generating X-ray and UV auroral flares.

Acknowledgement:

The work was supported by the National Science Foundation of China (41704169, 41525016, 41474155, 41274167). Z. Y., D. G. and B. P. acknowledge financial support from the Belgian Federal Science Policy Office (BELSPO) via the PRODEX Programme of ESA. L.C.R. was funded by an STFC Consolidated Grant to Lancaster University (ST/R000816/1). Cassini operations are supported by NASA (managed by the Jet Propulsion Laboratory) and ESA. The data presented in this paper are available from the NASA Planetary Data System http://pds-ppi.igpp.ucla.edu/.

References:

Angelopoulos, V., et al. 2008, Science, 321, 931

Arridge, C. S., et al. 2016, Nature Physics, 268

Azari, A. R., et al. 2018, Journal of Geophysical Research: Space Physics, 123, 4692

Badman, S. V., et al. 2015, Space Science Reviews, 187, 99

Badman, S. V., et al. 2013, Geophysical Research Letters, 40, 1027

Bagenal, F., Wilson, R. J., Siler, S., Paterson, W. R., & Kurth, W. S. 2016, Journal of Geophysical Research: Planets

Blanc, M., et al. 2015, Space Science Reviews, 192, 237

Delamere, P., Otto, A., Ma, X., Bagenal, F., & Wilson, R. 2015, Journal of Geophysical Research: Space Physics, 120, 4229

Dougherty, M. K., et al. 2004, Space Science Reviews, 114, 331

Drake, J., Swisdak, M., Che, H., & Shay, M. 2006, Nature, 443, 553

Dungey, J. W. 1961, Physical Review Letters, 6, 47

Egedal, J., Daughton, W., & Le, A. 2012, Nature Physics, 8, 321

Guo, R., et al. 2018, Nature Astronomy, 2, 640

Hesse, M., Chen, L., Liu, Y.-H., Bessho, N., & Burch, J. 2017, Physical review letters, 118, 145101

Hones, E. W. 1979, Space Science Reviews, 23, 393

Huddleston, D. E., Russell, C. T., Le, G., & Szabo, A. 1997, Journal of Geophysical Research: Space Physics, 102, 24289

Jackman, C., Slavin, J., & Cowley, S. 2011, Journal of Geophysical Research: Space Physics, 116, A10212

Kronberg, E., Glassmeier, K. H., Woch, J., Krupp, N., Lagg, A., & Dougherty, M. 2007, Journal of Geophysical Research: Space Physics, 112

Liang, H., Lapenta, G., Walker, R. J., Schriver, D., El-Alaoui, M., & Berchem, J. 2017, Journal of Geophysical Research: Space Physics, 122, 618

Masters, A. 2017, Journal of Geophysical Research: Space Physics, 122, 11

McAndrews, H., Owen, C., Thomsen, M., Lavraud, B., Coates, A., Dougherty, M., & Young, D. 2008, Journal of Geophysical Research: Space Physics, 113, A04210

Mitchell, D., et al. 2009, Planetary and Space Science, 57, 1732

Palmaerts, B., Radioti, A., Roussos, E., Grodent, D., Gérard, J. C., Krupp, N., & Mitchell, D. G. 2016b, Journal of Geophysical Research: Space Physics, 121, 11

Palmaerts, B., Roussos, E., Krupp, N., Kurth, W. S., Mitchell, D. G., & Yates, J. N. 2016a, Icarus, 271, 1

Paschmann, G., et al. 1979, Nature, 282, 243

Radioti, A., Woch, J., Kronberg, E. A., Krupp, N., Lagg, A., Glassmeier, K.-H., & Dougherty, M. K. 2007, Journal of Geophysical Research: Space Physics, 112, A06221

Roussos, E., et al. 2016, Icarus, 263, 101

Sergis, N., et al. 2011, Journal of Geophysical Research: Space Physics, 116

Sergis, N., et al. 2013, Journal of Geophysical Research: Space Physics, 118, 1620

Slavin, J. A., et al. 2009, science, 324, 606

Vasyliunas, V. 1983, Physics of the Jovian magnetosphere, 1, 395

Wang, S., Chen, L. J., Bessho, N., Kistler, L. M., Shuster, J. R., & Guo, R. 2016, Journal of Geophysical Research: Space Physics, 121, 2104

Yao, Z., et al. 2017, The Astrophysical Journal Letters, 846, L25

Yates, J. N., et al. 2016, Geophysical Research Letters, 43, 11

Young, D., et al. 2004, Space Science Reviews, 114, 1

Zweibel, E. G., & Yamada, M. 2009, Annual review of astronomy and astrophysics, 47, 291

Figure 1. Dayside magnetodisc reconnection event on 25 November 2005. (a) Three magnetic field components in KRTP coordinates (B_r in blue, B_θ in green and B_φ in red), and (b) in reconnection coordinates (B_X in blue, B_Y in green and B_Z in red). (c) Energetic electron differential flux from MIMI-LEMMS. (d) Energy spectrogram of omni-directional electron flux from CAPS-ELS. (e-g) Pitch angle distribution for electrons within energy ranges of from 50 eV to 500 eV, 500 eV to 3 keV, and 3 keV to 28 keV. (h) Energetic proton differential flux from MIMI-LEMMS. (i) Energy spectrogram for omni-directional ion flux from CAPS-IMS. (j) Energetic oxygen differential flux from MIMI-INCA. The pink regions highlighted the two reconnection regions that are identified by combining the signatures of negative B_θ component, Hall magnetic field, and the heated electrons.

Figure 2. Dayside magnetodisc reconnection event on 15 September 2008. The panels are arranged as the same format as Figure 1. The high electron/ion fluxes from C0/A0 channel at the beginning of Figure 2c/2h are due to light contamination.

Figure 3. Dayside magnetodisc reconnection event on April 14th and April 15th in 2008. The panels are arranged as the same format as Figure 1 and Figure 2. The four coloured arrows show the correspondence between the B_r dips and the low energy electron bands.

Figure 4. Differential flux and energy spectrogram for the energetic protons (a-b) and energetic oxygen (c-d) from MIMI-INCA on November 25, 2005, i.e., the first event. There are two major peaks for both protons and oxygen. The fluxes across all energies are enhanced at 13:04 and 13:18 simultaneously.

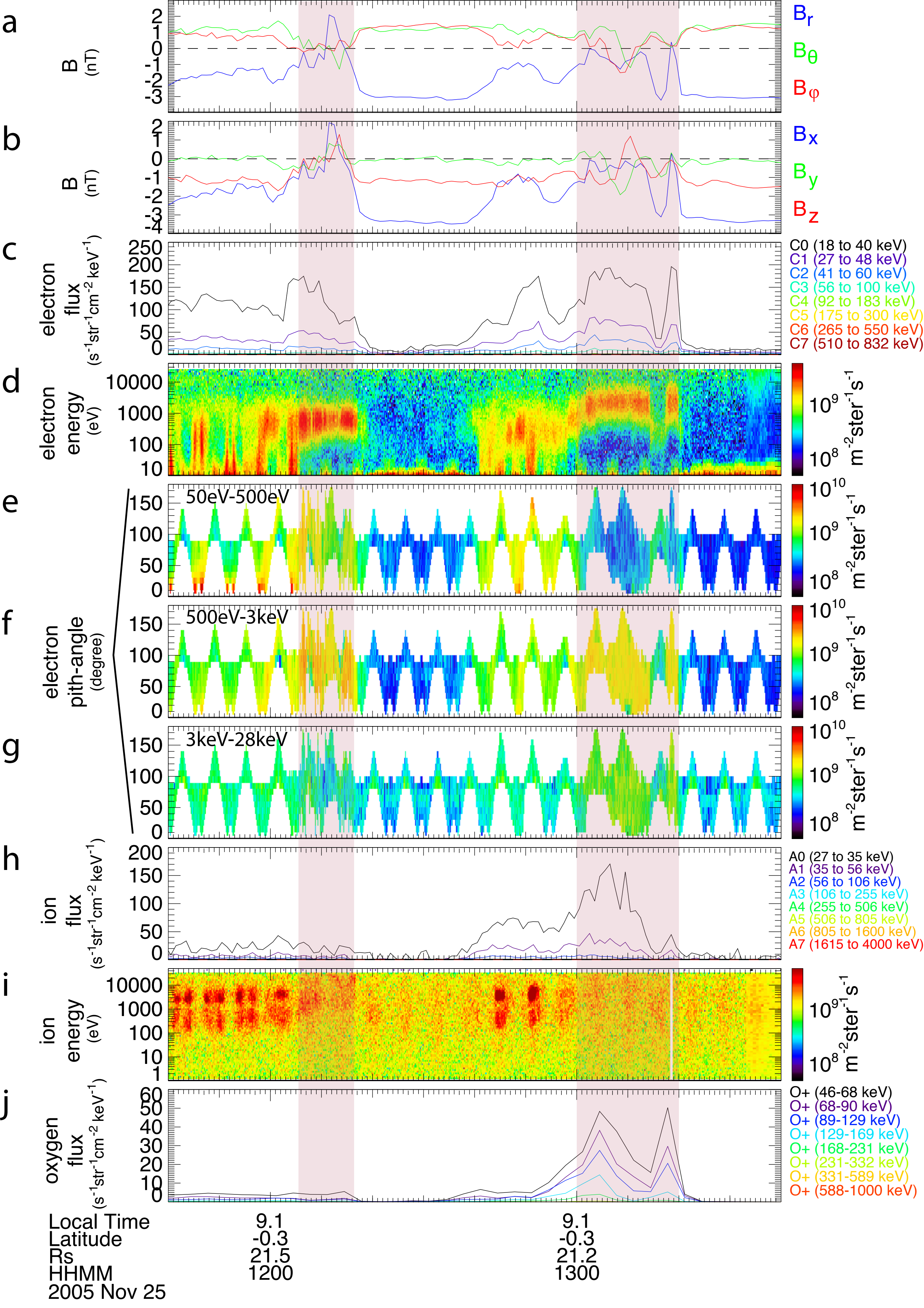
a
B (nT)
B_r
B_θ
B_φ
b
B (nT)
B_x
B_y
B_z
c
electron flux ($s^{-1}str^{-1}cm^{-2}keV^{-1}$)
C0 (18 to 40 keV)
C1 (27 to 48 keV)
C2 (41 to 60 keV)
C3 (56 to 100 keV)
C4 (92 to 183 keV)
C5 (175 to 300 keV)
C6 (265 to 550 keV)
C7 (510 to 832 keV)
d
electron energy (eV)
$m^{-2}ster^{-1}s^{-1}$
e
50eV-500eV
f
500eV-3keV
g
3keV-28keV
electron pith-angle (degree)
h
ion flux ($s^{-1}str^{-1}cm^{-2}keV^{-1}$)
A0 (27 to 35 keV)
A1 (35 to 56 keV)
A2 (56 to 106 keV)
A3 (106 to 255 keV)
A4 (255 to 506 keV)
A5 (506 to 805 keV)
A6 (805 to 1600 keV)
A7 (1615 to 4000 keV)
i
ion energy (eV)
j
oxygen flux ($s^{-1}str^{-1}cm^{-2}keV^{-1}$)
O+ (46-68 keV)
O+ (68-90 keV)
O+ (89-129 keV)
O+ (129-169 keV)
O+ (168-231 keV)
O+ (231-332 keV)
O+ (331-589 keV)
O+ (588-1000 keV)
Local Time 9.1 9.1
Latitude -0.3 -0.3
Rs 21.5 21.2
HHMM 1200 1300
2005 Nov 25

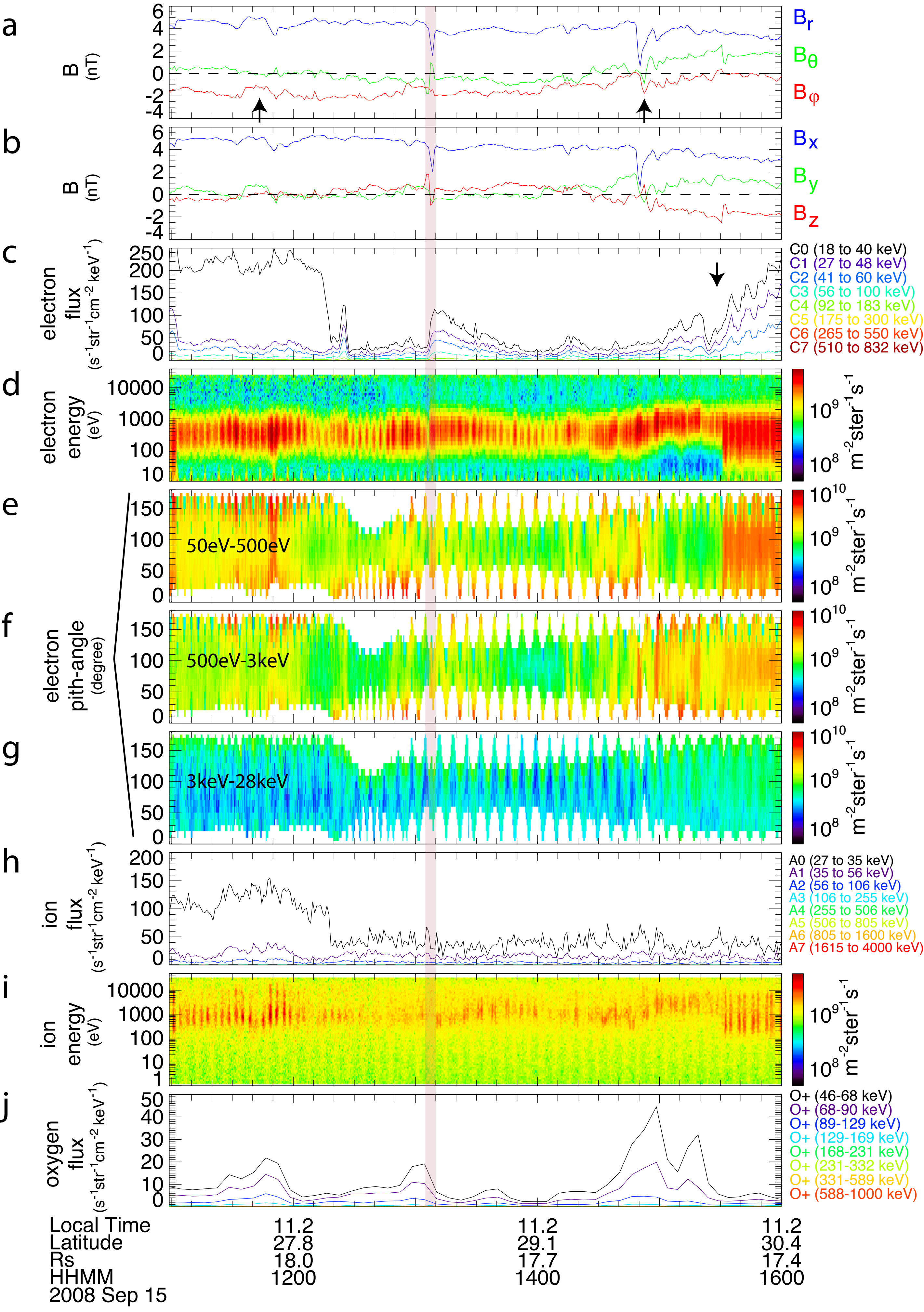

a
B (nT)
B_r
B_θ
B_φ
b
B (nT)
B_x
B_y
B_z
c
electron flux ($s^{-1}str^{-1}cm^{-2}keV^{-1}$)
C0 (18 to 40 keV)
C1 (27 to 48 keV)
C2 (41 to 60 keV)
C3 (56 to 100 keV)
C4 (92 to 183 keV)
C5 (175 to 300 keV)
C6 (265 to 550 keV)
C7 (510 to 832 keV)
d
electron energy (eV)
$m^{-2}ster^{-1}s^{-1}$
e
electron pith-angle (degree)
50eV-500eV
f
500eV-3keV
g
3keV-28keV
h
ion flux ($s^{-1}str^{-1}cm^{-2}keV^{-1}$)
A0 (27 to 35 keV)
A1 (35 to 56 keV)
A2 (56 to 106 keV)
A3 (106 to 255 keV)
A4 (255 to 506 keV)
A5 (506 to 805 keV)
A6 (805 to 1600 keV)
A7 (1615 to 4000 keV)
i
ion energy (eV)
j
oxygen flux ($s^{-1}str^{-1}cm^{-2}keV^{-1}$)
O+ (46-68 keV)
O+ (68-90 keV)
O+ (89-129 keV)
O+ (129-169 keV)
O+ (168-231 keV)
O+ (231-332 keV)
O+ (331-589 keV)
O+ (588-1000 keV)
Local Time 11.2 11.2 11.2
Latitude 27.8 29.1 30.4
Rs 18.0 17.7 17.4
HHMM 1200 1400 1600
2008 Sep 15

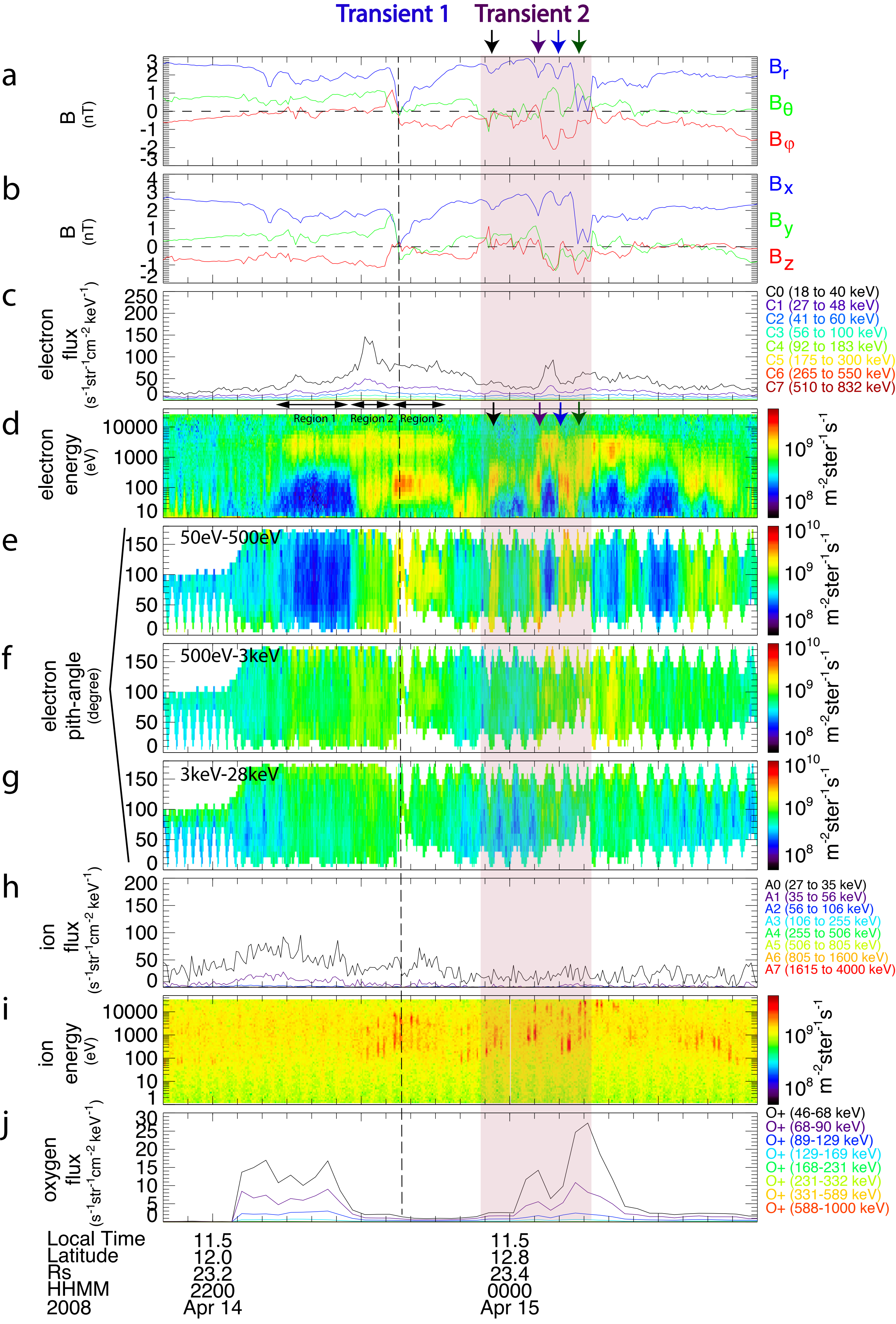

Transient 1
Transient 2
a
B (nT)
Br
Bθ
Bφ
b
B (nT)
Bx
By
Bz
c
electron flux (s-1str-1cm-2keV-1)
C0 (18 to 40 keV)
C1 (27 to 48 keV)
C2 (41 to 60 keV)
C3 (56 to 100 keV)
C4 (92 to 183 keV)
C5 (175 to 300 keV)
C6 (265 to 550 keV)
C7 (510 to 832 keV)
d
electron energy (eV)
Region 1
Region 2
Region 3
m-2ster-1s-1
e
50eV-500eV
f
500eV-3keV
g
3keV-28keV
electron pith-angle (degree)
h
ion flux (s-1str-1cm-2 keV-1)
A0 (27 to 35 keV)
A1 (35 to 56 keV)
A2 (56 to 106 keV)
A3 (106 to 255 keV)
A4 (255 to 506 keV)
A5 (506 to 805 keV)
A6 (805 to 1600 keV)
A7 (1615 to 4000 keV)
i
ion energy (eV)
j
oxygen flux (s-1str-1cm-2 keV-1)
O+ (46-68 keV)
O+ (68-90 keV)
O+ (89-129 keV)
O+ (129-169 keV)
O+ (168-231 keV)
O+ (231-332 keV)
O+ (331-589 keV)
O+ (588-1000 keV)
Local Time 11.5 11.5
Latitude 12.0 12.8
Rs 23.2 23.4
HHMM 2200 0000
2008 Apr 14 Apr 15

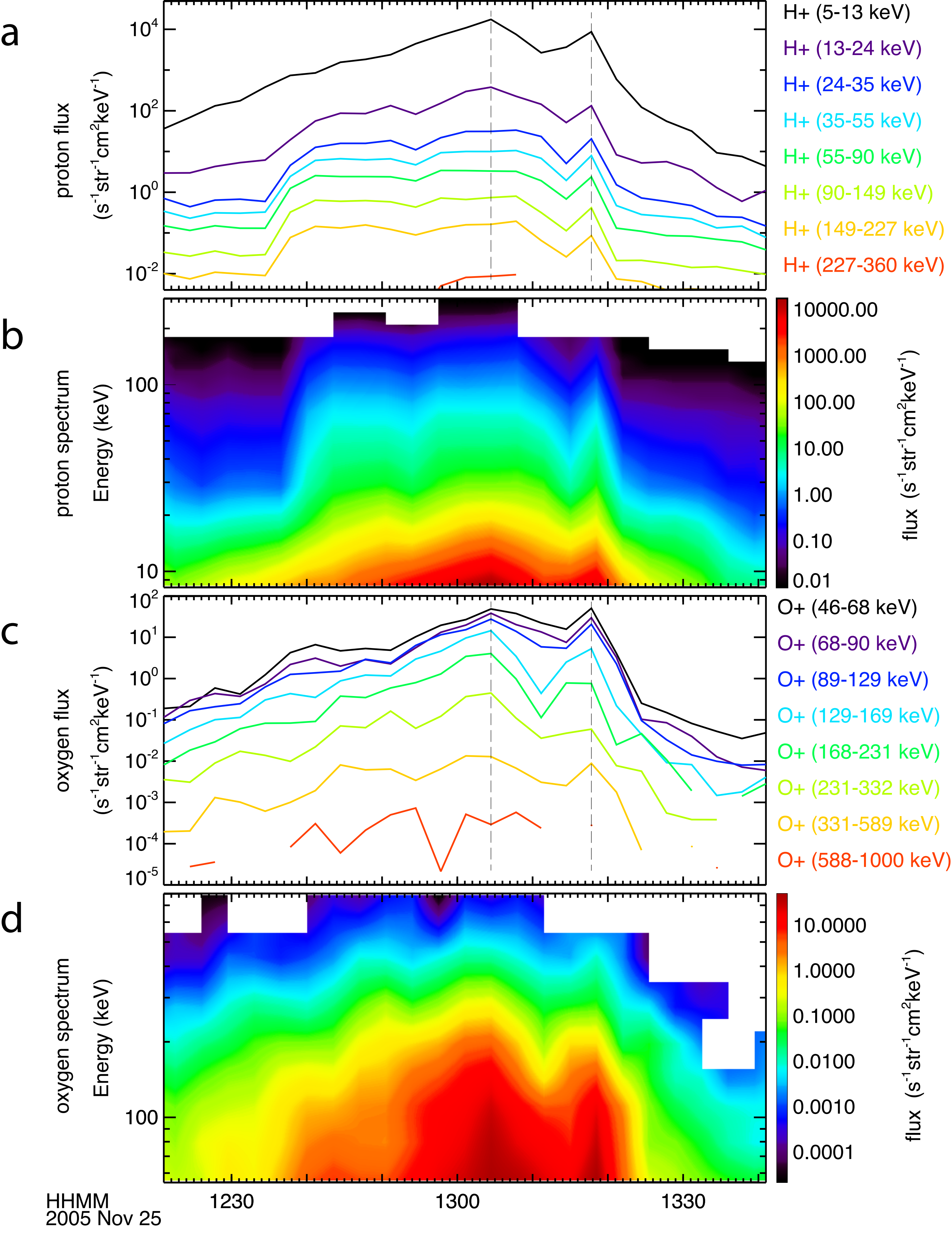

a
b
c
d
proton flux
(s-1str-1cm2keV-1)
H+ (5-13 keV)
H+ (13-24 keV)
H+ (24-35 keV)
H+ (35-55 keV)
H+ (55-90 keV)
H+ (90-149 keV)
H+ (149-227 keV)
H+ (227-360 keV)
proton spectrum
Energy (keV)
flux (s-1str-1cm2keV-1)
10000.00
1000.00
100.00
10.00
1.00
0.10
0.01
oxygen flux
(s-1str-1cm2keV-1)
O+ (46-68 keV)
O+ (68-90 keV)
O+ (89-129 keV)
O+ (129-169 keV)
O+ (168-231 keV)
O+ (231-332 keV)
O+ (331-589 keV)
O+ (588-1000 keV)
oxygen spectrum
Energy (keV)
flux (s-1str-1cm2keV-1)
10.0000
1.0000
0.1000
0.0100
0.0010
0.0001
HHMM
2005 Nov 25
1230
1300
1330